






# How Small-scale Jetlike Solar Events from Miniature Flux Rope Eruptions Might Produce the Solar Wind

Alphonse C. Sterling<sup>1</sup> , Navdeep K. Panesar<sup>2,3</sup> , and Ronald L. Moore<sup>1,4</sup> 

<sup>1</sup>NASA/Marshall Space Flight Center, Huntsville, AL 35812, USA

<sup>2</sup>Bay Area Environmental Research Institute, NASA Research Park, Moffett Field, CA 94035, USA

<sup>3</sup>Lockheed Martin Solar and Astrophysics Laboratory, 3251 Hanover Street, Building 252, Palo Alto, CA 94304, USA

<sup>4</sup>Center for Space Plasma and Aeronomic Research, University of Alabama in Huntsville, Huntsville, AL 35805, USA

Received 2023 October 31; revised 2024 January 5; accepted 2024 January 9; published 2024 February 21

## Abstract

We consider small-scale jetlike events that might make the solar wind, as has been suggested in recent studies. We show that the events referred to as “coronal jets” and as “jetlets” both fall on a power-law distribution that also includes large-scale eruptions and spicule-sized features; all of the jetlike events could contribute to the solar wind. Based on imaging and magnetic field data, it is plausible that many or most of these events might form by the same mechanism: Magnetic flux cancelation produces small-scale flux ropes, often containing a cool-material minifilament. This minifilament/flux rope erupts and reconnects with adjacent open coronal field, along which “plasma jets” flow and contribute to the solar wind. The erupting flux ropes can contain twist that is transferred to the open field, and these become Alfvénic pulses that form magnetic switchbacks, providing an intrinsic connection between switchbacks and the production of the solar wind.

*Unified Astronomy Thesaurus concepts:* [Solar filament eruptions \(1981\)](#); [Solar extreme ultraviolet emission \(1493\)](#); [Solar magnetic fields \(1503\)](#); [Solar wind \(1534\)](#)

## 1. Introduction

With the advent of fresh data from satellites in the near-Sun heliosphere, there is renewed interest in the possibility that small-scale eruptions might be the cause of the pervasive solar wind outflow. Raouafi et al. (2023) suggest that small-scale jetlike outflows, called jetlets, might be the primary responsible agent. EUV images show that jetlets have widths of a few thousand kilometers and are extremely abundant over the entire quiet and coronal hole Sun. Different from active regions, they are present throughout the solar cycle, as is the solar wind.

Raouafi et al. (2023) further speculated that a subset of the copious small-scale magnetic cancelation episodes occurring in the photosphere are responsible for driving the jetlet production through magnetic reconnection. They argue that their estimated rate of  $5 \times 10^5$  jetlets day<sup>-1</sup> would be sufficient to supply the mass and energy requirements of the solar wind. Furthermore, they argue that the magnetic switchbacks, which are localized rotations in the solar wind magnetic field that are ubiquitously detected in near-Sun Parker Solar Probe (PSP) data, could also be a consequence of the magnetic reconnection events that produce the jetlets and solar wind and are built up and triggered by fine-scale flux cancelation.

Chitta et al. (2023), on the other hand, use Solar Orbiter data to conclude that there are even smaller-scale features, which they call “picoflare jets,” with widths  $\sim 100$  km. These observations are of a coronal hole using Solar Orbiter’s EUV High Resolution Imager (HRI<sub>EUV</sub>) at 174 Å and were taken during a close approach of 0.332 au, where the images had a spatial resolution of about 237 km. Based on their morphology, they suggest that these picoflare jets are driven by magnetic reconnection. Based on the number of events that they

observed, and extrapolating the filling factor of the jets over the area they observed to the entire Sun, they estimate that the picoflare jets might account for 20% of the solar wind mass flux.

Both of these studies present observations in support of small-scale jetlike events (which we will call “small-scale jets”) providing mass and energy to the solar wind. In this work, we present a picture for how the small-scale jets come from built-up magnetic energy, are generated, produce outflows, and can propagate into the solar wind and often form switchbacks. We also speculate on how these small-scale jets could contribute mass and heating to the solar wind.

A previous study, Moore et al. (2011), also suggested that small-scale jets could lead to generation of the solar wind and the entire heliosphere, but they took those jets to be type II spicules. This work updates the concept of that idea, based on much new information that we have gained on jets and jetlike features, and we consider other subsequently discovered jetlike features than spicules (e.g., jetlets), although spicules might still be a contributing component. That older (Moore et al. 2011) work was based on previous ideas for how X-ray coronal jets were thought to form at the time, namely via emerging magnetic field reconnecting with surrounding ambient coronal field (Shibata et al. 1992; Yokoyama & Shibata 1995). Much evidence now supports that coronal jets are instead produced by small-scale filament (minifilament) eruptions, and that those minifilament eruptions are at least often a consequence of magnetic flux cancelation.

## 2. Coronal Jets

Coronal jets are usually observed at soft X-ray (SXR) and/or EUV wavelengths. In SXR images, jets reach about 50,000 km with widths  $\sim 8000$  km, based on observations from Hinode’s X-Ray Telescope (XRT) by Savcheva et al. (2007). Extrapolating their values of 60 jets day<sup>-1</sup> in the two coronal holes

yields an occurrence rate of a few hundred per day over the entire solar surface for the size and quality of jets that they observed in that wavelength band. They have lifetimes of from about 10 to 30 minutes, and estimates for the energy expended in coronal jets range over  $\sim 10^{26}$ – $10^{29}$  erg (e.g., Raouafi et al. 2016; Hinode Review Team et al. 2019; Sterling et al. 2023).

Sterling et al. (2015) argued that essentially all jets result from the eruption of a minifilament. These minifilaments are frequently seen in absorption in Solar Dynamics Observatory (SDO) Atmospheric Imaging Assembly (AIA) EUV images, often including in the He II  $\lambda 304$  channel, indicating that they are likely cool (chromospheric-temperature) features that can reside in the low corona, a la typical filaments. In the following, we describe jet production in an open magnetic field environment, since we are focusing on jets that might contribute to the solar wind. This obviously applies to a coronal hole environment, although the same arguments can be extended to quiet-Sun and even active regions (Panesar et al. 2016b; Sterling et al. 2024).

In an open-field location such as a coronal hole, the background field will largely be unipolar, consisting of a single majority polarity. The minifilament forms at a location where a minority-polarity flux patch resides inside of the sea of surrounding majority polarity, with the resulting magnetic topology being that of an anemone region (Shibata et al. 2007); that is, the minority polarity fans out into a three-dimensional lobe connecting to the surrounding majority-polarity field, with a magnetic null point elevated above the minority flux patch, and with the surrounding coronal field forming a pseudostreamer magnetic configuration as the envelope of the anemone. The basic schematic for the process appears in Sterling et al. (2015) (also see the figures in Section 6, below). In this two-dimensional sketch, the anemone’s base appears as a double lobe (in the 2D cross section). Prior to eruption, the minifilament sits in one of the lobes, along a magnetic neutral line between the majority and minority polarities. Because the minifilament looks like a scaled-down version of a typical solar filament, Sterling et al. (2015) assumed that upon eruption the cool minifilament material would be wrapped inside of an erupting minifilament magnetic flux rope. It is this flux rope eruption that is key to the jet formation, although the cool minifilament material is vital to understanding the evolution of that field leading to and during the eruption.

Upon eruption, the minifilament/flux rope is expelled toward the null over the minority polarity and undergoes reconnection with the far-side ambient coronal field. This reconnection is of the “interchange” variety, which was called *external reconnection* in Sterling et al. (2015), with previously closed field of the flux rope becoming new open field along the pseudostreamer spire and becoming new closed field over the lobe of the anemone opposite to where the minifilament eruption originated; this outflowing heated material becomes the spire of the jet that is observed in SXR and/or EUV. If the minifilament/flux rope erupts far enough, the external reconnection can erode away enough of the enveloping flux rope field so that the cool minifilament material can also escape and flow outward along the spire; this results in a cool component to the jet, often seen in AIA 304 Å images (Moore et al. 2010, 2013). Eruptions of miniature filaments at the start of jets had been seen in previous investigations also (e.g., Nisticò et al. 2009; Shen et al. 2012; Adams et al. 2014).

About concurrent with (or slightly before or slightly after; see Moore et al. 2018) the external reconnection, *internal reconnection* also occurs among the legs of the erupting minifilament field that are still rooted in the solar surface. This corresponds to the flare-producing reconnection below typical erupting filaments. In the case of the erupting minifilament, a strong brightening is often apparent in SXRs, occurring off to the side of the jet base from which the minifilament erupts. This brightening, first identified by Shibata et al. (1992), was identified as a miniature flare by Sterling et al. (2015), who called the feature a jet bright point (JBP).

Panesar et al. (2016b) examined the cause of jet-producing minifilament eruptions by tracking the magnetic base of 10 on-disk quiet-Sun jets that were observed in AIA images. Using SDO/Heliographic and Magnetic Imager (HMI) magnetograms, they found that in all their cases flux cancellation occurred in the jet base before and during the jetting time. Similarly, Panesar et al. (2018a) studied 13 on-disk coronal hole jets and again found pre-eruption and during-eruption flux cancellation to occur at the jet locations. These findings are consistent with results from several earlier single-event studies (e.g., Shen et al. 2012; Young & Muglach 2014b, 2014a; Adams et al. 2014) and also with several later studies (McGlasson et al. 2019; Chen et al. 2020; Muglach 2021). Thus, there is strong evidence that cancellation leads to at least a substantial portion of coronal jets.

Coronal jets, then, are smaller-scale analogs to larger-scale typical solar eruptions. While large-scale filaments erupt to make a typical solar flare and often a coronal mass ejection (CME), minifilaments erupt to make a JBP and a jet spire. Sterling et al. (2018) have examined this issue from the other direction by presenting evidence that relatively magnetically isolated CME-producing eruptions do indeed appear to behave as larger-scale jet-producing minifilament eruptions.

Several studies indicate that jets show spinning motion as they extend outward from the surface, including Patsourakos et al. (2008), Raouafi et al. (2010), Sterling et al. (2010), Chen et al. (2012), Curdt et al. (2012), Morton et al. (2012), Shen et al. (2012), Hong et al. (2013), Joshi et al. (2018), Zhelyazkov & Chandra (2018), Liu et al. (2019), and Panesar et al. (2022). This twisting/untwisting motion has been supported with spectroscopic studies also (Pike & Mason 1998; Kamio et al. 2010). Wang & Sheeley et al. (1998) found that some jets can persist well into the corona, manifesting in white-light coronagraphs as “white-light jets,” which are sometimes called “narrow CMEs” (Sterling 2018). Moore et al. (2015) found that the jets from which the white-light jets originated were ones that tended to have a larger amount of untwisting as they ascended, as measured using AIA 304 Å movies, and they also found evidence that the (un)twisting of the jets persisted as an oscillatory swaying movement of the white-light jets.

We can synthesize the flux cancellation and jet rotation into the minifilament eruption picture for jets as follows: The flux cancellation results in the formulation of a magnetic flux rope. If conditions are appropriate, then a cool-material minifilament forms along that flux rope (see Panesar et al. 2017). If the cancellation occurs along a sheared-field neutral line, then that shear can be converted into twist in the resulting minifilament/flux rope (van Ballegooijen & Martens 1989). As the cancellation continues (or the cancellation might resume after it had paused; Panesar et al. 2017), the flux rope becomes unstable and erupts outward, leading to the jet as described

above. The twist of the flux rope can then be transmitted to the open field through the external reconnection, following a process described by Shibata & Uchida (1986).

Several reviews and summaries of jets are now available (Shimojo & Shibata 2000; Shibata & Magara 2011; Raouafi et al. 2016; Hinode Review Team et al. 2019; Shen 2021; Sterling 2021; Schmieder 2022; Sterling et al. 2023).

### 3. Jetlets

Raouafi & Stenborg (2014) identified features in AIA 171 and 193 Å movies that appeared similar to coronal jets, but of shorter durations—tens of seconds to a few minutes—and of smaller size than typical coronal jets. That study found these jetlets to be obvious at the base of solar coronal plumes.

Panesar et al. (2018b) also studied jetlets, using both AIA EUV images and UV images from the Interface Region Imaging Spectrograph (IRIS) satellite. They found the jetlets to appear in more general network regions rather than just at the base of plumes and to have typical lengths of  $\sim 27,000$  km, widths of 3000 km, and lifetimes of 3 minutes. Using high-resolution ( $0''.129$  pixels, compared to, e.g.,  $0''.6$  pixels for AIA) Hi-C2.1 EUV 172 Å images (Rachmeler et al. 2019), Panesar et al. (2019) observed six jetlets that were of even smaller size: about 9000 km in length and 600 km in width. These Hi-C jetlets also were rooted at the edges of magnetic network lanes.

Raouafi et al. (2023) estimated the rate of energy expenditure of a jetlet to be  $\sim 5 \times 10^{22}$  erg  $s^{-1}$ . Assuming lifetimes of 20 s to 5 minutes (see Raouafi & Stenborg 2014; Panesar et al. 2018b), this gives a total energy of  $\sim 10^{24}$ – $10^{25}$  erg for a single jetlet.

All four of the studies, Raouafi & Stenborg (2014), Panesar et al. (2018b, 2019), and Raouafi et al. (2023), used magnetograms to investigate the magnetic behavior at the base of the jetlets, and all found evidence that magnetic cancellation episodes were closely tied to jetlet formation. For example, Raouafi & Stenborg (2014) conclude that the jetlets result from “flux emergence followed by magnetic cancellation of the minority polarity with the dominant unipolar field concentration.” From a study of 10 jetlets, Panesar et al. (2018b) found clear evidence for flux cancellation preceding nine of them, with an average rate of about  $1.5 \times 10^{18}$  Mx  $hr^{-1}$ . Panesar et al. (2019) found that four of their six jetlet-like events resulted from flux cancellation.

Furthermore, Panesar et al. (2018b, 2019) argued that jetlets are analogs of the larger-scale coronal jets discussed in Section 2. Jetlets are similar to coronal jets in that they appear jetlike, namely, with a bright base and a spire that extends in time. Moreover, their extension velocity in EUV is  $\sim 70$  km  $s^{-1}$ , which is similar to the corresponding coronal jet value of  $\sim 100$  and  $70$  km  $s^{-1}$  for quiet-Sun and coronal hole jets, respectively (Panesar et al. 2016a, 2018a, 2018b). The flux cancellation at the base of jetlets mimics that for many jets. Also similar to jets, some jetlets might display twisting motion (Panesar et al. 2018b, 2019), although these observations are at the limit of detection and therefore not conclusive.

Despite searching for erupting minifilaments at the base of jetlets, however, the Panesar et al. studies did not find any. This could well be due to the small size of the features. Even in jets, erupting minifilaments can be difficult to detect in the smaller and less distinct ones, especially the so-called “standard jets”; these are jets with relatively narrow spires, compared to the size

of the same jet’s base region, especially when observed in SXR (Moore et al. 2010, 2013). These standard jets often form from erupting minifilaments that are confined to the base of the jet (Sterling et al. 2022a) and thus would be more difficult to detect than in jets with erupting minifilaments that are ejected out along the jet’s spire (often forming “blowout jets,” which have broad spires compared to the base in SXR). Kumar et al. (2022), however, did report observing a minifilament that apparently is erupting in a jetlet that they report is about two times larger than a typical jetlet but smaller than typical jets.

Therefore, it might be that higher-resolution EUV imaging (Sterling et al. 2023) will be required to confirm the presence of erupting minifilaments in most jetlets. With this caveat, then, we regard the above-noted similarities between jetlets and coronal jets as evidence that jetlets are smaller-scale versions of coronal jets.

### 4. Smaller Jetlike Features

If jetlets are indeed small-scale jets, then jetlike features likely occur on still smaller size/energy scales also.

Higher-resolution instruments should reveal such features, if they exist. Indeed, Solar Orbiter identified small-scale features dubbed “campfires” (Berghmans et al. 2021; Zhukov et al. 2021). These features are described as small-scale, short-lived coronal brightenings that can appear to be looplike, dotlike, or complex structures and that live for 1–60 minutes.

Panesar et al. (2021) studied 52 random campfires and concluded that they are “rooted at the the edge of photospheric [magnetic flux] lanes,” that most appear above magnetic neutral lines between opposite-polarity magnetic patches, and that most of them are “preceded by a cool-plasma structure, analogous to minifilaments in coronal jets.” They also conclude that some of the campfires appear similar to coronal jets. From their table of 52 events, they list nine of them as appearing jetlike. Culling out the properties of these nine, we find that those jetlike campfires have lengths of  $5500 \pm 2300$  km. This is not far different from the statistics on all 52 given in Panesar et al. (2021),  $4500 \pm 2500$  km, and so this indicates that the remaining 43 events that are not classified as “jetlike” may be fundamentally similar. These lengths are somewhat smaller than the average values for jetlets, and therefore they could be part of a population of smaller-sized objects that operate via the same mechanism as jets. The dark feature visible in them appears to be an erupting minifilament, like those seen in coronal jets.

Figure 1 shows images of a jetlike campfire from the Solar Orbiter Extreme Ultraviolet Imager (EUI) High Resolution Imager HRI<sub>EUV</sub>, at 174 Å. This is event 13 in Panesar et al. (2021; see their Figure 6). Arrows in the figure point out the erupting dark feature. This feature is also prominent in absorption in AIA 304, 171, and 193 Å images, suggesting that it is composed of cool material, and clearly is erupting in this sequence (animations are available in Panesar et al. 2021). The look and dynamics of this absorbing feature are essentially identical to the minifilaments that erupt to make coronal jets, and therefore this is in all likelihood an event occurring via the same jet-producing mechanism, but on a size scale smaller than that of typical jets.

The Solar Orbiter-observed picoflare jets of Chitta et al. (2023) are much smaller still, with spatial scales of  $\sim$ few  $\times$  100 km, which is comparable to the widths of spicules. They estimate a lower limit of the kinetic energy to be  $\sim 10^{21}$  erg for

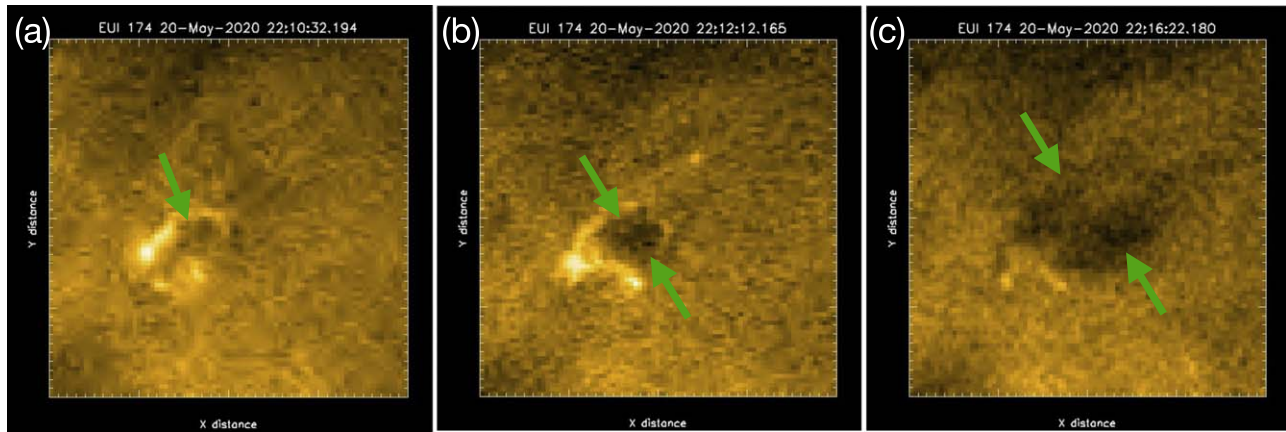


**Figure 1.** Solar Orbiter EUV HRI<sub>EUV</sub> 174 Å images of a “campfire,” as reported by Panesar et al. (2021). Arrows show an absorption feature in the process of erupting. The eruption is essentially identical to the minifilament eruptions that make coronal jets. This is likely cool-temperature material, due to its prominent visibility in cool SDO/AIA channels (Panesar et al. 2021, Figure 6). In this case, the cool material is expelled from the campfire location through panels (a), (b), and (c). For both axes, each minor tick represents a distance of about 725 km.

the picoflare jets. Spicules might require  $\sim 10^{25}$  erg, but that is based on estimates for the gravitational energy (Sterling 2000), and so a direct comparison with the quoted picoflare energy value is likely not appropriate.

Sterling & Moore (2016) and Sterling et al. (2020) discuss in some detail the possibility that some spicules might be made by the coronal jet mechanism (also see Samanta et al. 2019). Spicules have morphological differences with coronal jets (and jetlets), however. For example, a bright base, common in the jetlike features, is not obvious in spicules, although it is possible that the internal reconnection responsible for that brightening in the jets does occur at the base of the spicules, but not enough photons are able to radiate through the dense chromosphere for a brightening to appear (Sterling et al. 2020).

In addition, there is as yet no convincing observation of an erupting minifilament at the base of spicules (although Sterling et al. 2020 point out candidate detections). Instead, most spicules seem to form very low down and appear as a spicular outflow at earliest detection. Some active region jets also have such an appearance, like geysers (Paraschiv & Donea 2019; Paraschiv et al. 2020, 2022). But nonetheless, in the active region jet case there is evidence that they do indeed result from minifilament eruptions, but where the external reconnection occurs at a low altitude and is often obscured by surrounding elevated low-atmosphere material (Sterling et al. 2024). Similarly, an erupting putative *microfilament* might make spicules but be hidden by surrounding chromospheric material. Future observations, perhaps assisted by numerical simulations, will be required to determine whether the coronal jet mechanism makes some or most spicules, or if they are created instead by one or more different mechanisms (e.g., Iijima & Yokoyama 2017; Martínez-Sykora et al. 2017; Kotani & Shibata 2020).

## 5. Size Distributions of Erupting Filament-like Features, Revisited

Because jets appear to be caused by smaller-scale versions of filament eruptions that make typical solar flares and CMEs, Sterling & Moore (2016) considered whether the jet production mechanism might also occur on smaller size scales, with a power-law-type distribution. They specifically addressed this in terms of whether the same mechanism might make some or

most solar spicules. They plotted the size of the erupting filament feature on the abscissa; the largest of these are the filament eruptions that make flares and CMEs, using available values for the sizes of filaments. The next smallest feature they plotted was for minifilaments that erupt to make jets, based on the sizes provided by Savcheva et al. (2007). For the size of the erupting microfilaments that they postulated might make spicules, they used measured values of spicule widths; this is because the widths of jet spires for polar coronal hole Hinode/XRT-observed jets are roughly in agreement with the size of the erupting minifilaments that made a different set of polar coronal hole Hinode/XRT-observed jets used in Sterling et al. (2015). For the ordinate, they plotted the estimated number of the events occurring on the entire Sun at any given time. Such estimates for spicules are available from historical studies. For jets, they estimated values using rates in polar coronal holes given by Savcheva et al. (2007). Similarly, flare and CME rates, along with flare durations, were used to make estimates for the number of large-scale eruptions occurring on the Sun at any time (Veronig et al. 2002; Yashiro et al. 2004; Chen 2011). Considering the extent of the ranges of the values for the measured or estimated quantities (which take the place of “error bars” on the plot), a best-fit line to all three of these points showed that those three values are consistent with following a power law. This shows that the idea that some percentage of spicules being made with the coronal jet mechanism is consistent with a power-law scaling of eruptions: eruptions of smaller filament-like features become more numerous as the size of the erupting feature gets smaller.

This idea was really based on an extension to smaller size scales of the filament-eruption mechanism making two types of features: typical flare- and CME-producing filament eruptions, and minifilament eruptions that make coronal jets. This is because, as mentioned earlier, spicules have some morphological differences from the larger eruptions, and also because erupting microfilaments have yet to be convincingly observed. There should, though, be other jetlike features between the coronal jets and spicules that could be added to the plot, since there is considerable size difference between the minifilaments that erupt to make jets ( $\sim 8000$  km) and the expected size of potential microfilaments that might erupt to make some spicules (a few 100 km). Jetlets fall into that intermediate size range. Until now there have not been reliable counts of the

possible number of jetlets on the Sun, but recently such an estimate has become available, and so we can add a new point to our size distribution plot.

We require the size of erupting minifilaments that might make jetlets. As discussed above (Section 3), there has been only one reported observation of an erupting minifilament making a jetlet (Kumar et al. 2022), but there have been observations of dark absorbing features in the jetlike campfires (Panesar et al. 2021), and those campfires are only slightly smaller than jetlets. Moreover, jetlets have morphological similarities to coronal jets and also have magnetic field behavior at their base that is similar to that of coronal jets (i.e., frequently showing cancellation). Therefore, it is plausible to speculate that many jetlets result from small minifilament eruptions. Again taking the size of those expected erupting minifilaments to be about the width of a jetlet spire, we merely have to consider the observed width of those spires. From Panesar et al. (2018b), the quoted range is  $3200 \pm 2000$  km. From Kumar et al. (2022), the quoted values are  $\sim 2''\text{--}3''$ . Panesar et al. (2019) observed smaller-sized jetlets with Hi-C's higher resolution and found spire widths of  $600 \pm 150$  km. Based on this, we adopt a range of values for the potential erupting minifilaments that might cause jetlets to be over the range 500–5000 km.

For the number of jetlets on the Sun, we rely on the values given in Raouafi et al. (2023). They looked at a fixed field of view (FOV) of  $70'' \times 70''$  magnetogram observations from Big Bear Solar Observatory's Goode Solar Telescope (BBSO/GST) and counted the number of cancellation events that they saw over that FOV (88) over an approximately 90-minute-long, nearly continuous observation period. During this time, they detected three EUV jetlets in the FOV. Extrapolating this to the entire Sun, Raouafi et al. (2023) concluded that there are six jetlets per second initiated over the entire Sun. If, as above (Section 3), we take the lifetime of jetlets to range between 20 and 300 s, then this yields a total number of jetlets on the Sun at any instant of 120–1800.

Figure 2 shows the resulting four-point plot, where the horizontal and vertical lines around the point represent the full extent of the abovementioned ranges for the erupting minifilament sizes and the total number of events on the Sun at any instant. The plotted solid line is the same fit as in Sterling & Moore (2016), that is, it is a best-fit line to the three points excluding the jetlets (i.e., the first, third, and fourth points, measured from left to right on the abscissa). Considering the range bars, the determined value for jetlets fits on this line. Therefore, the jetlets are consistent with fitting on the distribution of eruptive filament-like events, spanning large-scale eruptions that make typical solar flares and CMEs, down to some percentage of the spicules.

Recently, Uritsky et al. (2023) have published results of a quantitative investigation of the occurrence rate of coronal outflows involving 2300 events. They look at the size scale of the features leaving the Sun above a polar coronal hole in AIA 171 Å images over a 6 hr period. They find size scales (“transverse size”) of the outflows to range from the smallest detectable sizes up to  $\sim 4 \times 10^4$  km, and they show that the bulk of the outflows follow an approximate power-law distribution in their occurrence rate versus the sizes of the outflows. Our plot has a different vertical axis from theirs (we plot the number of erupting events on the Sun at a given time, while they plot the occurrence rate), and so we cannot make a

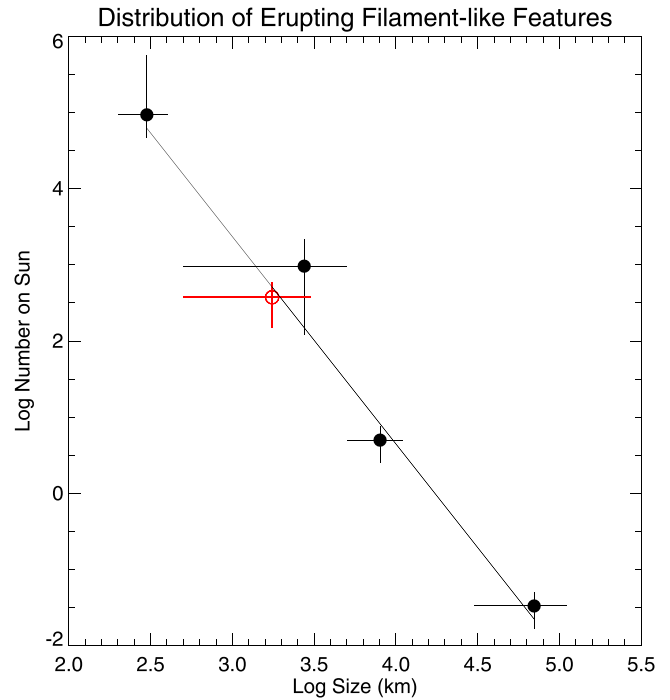


**Figure 2.** Augmentation of a plot in Sterling & Moore (2016), showing the number-against-size distribution of erupting filament-like features on the Sun. The horizontal axis shows the size (horizontal extent) of the erupting feature, and the vertical axis shows the number of events that are erupting on the Sun at any given instant in time. Among the black circle values, the point farthest to the right represents solar filaments erupting to make typical solar flares and CMEs, the second point from right represents the minifilaments erupting to make coronal jets, and the leftmost point represents the putative microfilaments erupting to make spicules or spicule-sized features. These three points were shown in Sterling & Moore (2016), and the solid line is a best fit to those three points. The fourth black circle, which is the second from the left, is a new addition that represents jetlets on the Sun, based on rate numbers from Raouafi et al. (2023) and the widths of jetlet spires from Panesar et al. (2018b, 2019) and Kumar et al. (2022). The red open circle represents the number of outflow events of about jetlet size occurring at a given time over the entire Sun, based on our estimates from the events observed by Uritsky et al. (2023) (see text). Rather than error bars, for each point the horizontal and vertical bars represent the approximate range of reported size and rate values, and the filled circle (or red circle) marks the middle of those ranges.

direct comparison of the distribution of events that they see with our results in Figure 2.

We can, however, crudely compare the Uritsky et al. (2023) event numbers with ours, by estimating the instantaneous number of their events that would be present over the entire Sun based on what they observe in their limited FOV. From Figure 5(b) of Uritsky et al. (2023), most of their 2300 events have a transverse size of between about 500 and 3000 km, based on the half-width of the transverse-size distribution plotted in that figure; we can use these values as range-bar lower and upper limits, and we take the value of 1750 km for our Figure 2 abscissa. For our ordinate, we have to estimate/guesstimate the number of Uritsky et al. (2023) events that would occur over the entire Sun at a given time. They observed 2300 events in 6 hr, from a portion of the solar limb that extends for 1/8 of the solar circumference. A substantial unknown, however, is from how far along the Earth–Sun line of sight the events observed above the limb by Uritsky et al. (2023) originate. That is, among the 2300 events observed in the plane of sky at the limb, some will originate from exactly at the limb, while others will originate from somewhat inside the

limb, and others will originate from somewhat beyond the limb; we do not know from how far inside and how far beyond the limb those features might originate and be observed in the observations of Figure 1(a) of Uritsky et al. (2023). To obtain a rough minimum estimate of the whole-Sun instantaneous number of events, we will assume that the maximum for this line-of-sight contribution region's extent is  $1/8$  of the circumference on either side of the limb. We can then approximate this source region of the Uritsky et al. (2023) features to be a two-dimensional rectangle with one side  $C_{\odot}/8$  in length (this is the along-the-limb width of the rectangle) and the other side  $C_{\odot}/4$  in length (the Earth-Sun line-of-sight length of the rectangle), where  $C_{\odot}$  is the solar circumference. The area of this rectangular region,  $C_{\odot}^2/(8 * 4)$ , is then  $\sim 1/10$  that of the surface area of the entire Sun. Thus, our minimum (lower limit) estimate for the number of events observed by Uritsky et al. (2023) over the entire Sun is  $2300 * 10 / 360 \text{ minute}^{-1}$ . From Figure 5(a) of Uritsky et al. (2023), the mean lifetime of their observed events is 2.6 minutes, and so the number of Uritsky et al. (2023) events seen at any one time on the entire Sun is  $\sim 2300 * 10 * 2.6 / 360 \sim 165$ . As a minimum estimate for the Earth-Sun line-of-sight length of the rectangle, we assume that the features observed by Uritsky et al. (2023) all come from only within  $C_{\odot}/32$  of the distance inside and beyond the limb, so that the line-of-sight side of the rectangle is now  $C_{\odot}/16$  in length; this yields an upper limit for the estimate for the number of events at any one time on the entire Sun of  $\sim 665$ . Using these extrema for the range-bar limits, and taking the value for the number of events (i.e., the point on the plot) to be the midpoint between those two extrema, we have a value of 415 events at any given time over the entire Sun. We plot this value based on Uritsky et al. (2023) as the open circle in our Figure 2. We see that this value is close to our plotted value (filled black circle) for jetlets in Figure 2.

Thus, although we have had to make some assumptions in extrapolating the Uritsky et al. (2023) features to the entire Sun, we can conclude that their observed features are broadly consistent with those features originating from jetlets. Moreover, the Uritsky et al. (2023) value provides an independent assessment for the number of outflowing features of the jetlet size scale, and this value is consistent with the value estimated from jetlet observations from Raouafi et al. (2023). Moreover, the two values from the Uritsky et al. (2023) work and the Raouafi et al. (2023) work are both consistent with the size distribution of the number of erupting-filament-like events on the Sun at any instant first presented in Sterling & Moore (2016).

## 6. Solar Wind Formation from Small-scale Eruptions that Make Jetlike Events

We can now posit how the solar wind might form from jetlike events, as proposed in Moore et al. (2011) and Raouafi et al. (2023). The latter work suggested that jetlets are the source of the solar wind. Our discussion above in Section 5, however, suggests that jetlets are part of a continuous distribution of eruptive events, from large-scale eruptions that make CMEs down to spicules (or spicule-sized features). Therefore, here we will describe the process as eruptions creating jetting events, where those events could be jets, jetlets, or smaller features.

Figure 3 summarizes different aspects of the process. All of the jetting events would evolve as described in Section 2 and as

shown in Figures 3(a)–(c). The magnetic flux rope that holds the erupting minifilament (represented by the blue circle in the figure) would form via magnetic cancellation in the photosphere (see Figure 4 in Panesar et al. 2016b). This process continues until the flux rope becomes destabilized and erupts. (Strictly speaking, a cool-material minifilament is not essential for this process. The miniature flux rope that forms could erupt even without such cool material, or with very little cool material on it. But the presence of the cool minifilament material allows us to infer the presence of the erupting field in EUV images.)

Figures 3(d)–(g) show a continuation of the evolution, with the external reconnection eroding away the entire outer envelope of the erupting minifilament. The twist of the erupting minifilament flux rope is thereby transmitted to the open field (Shibata & Uchida 1986), as mentioned in Section 2, and this twist can show up as swaying of the white-light jets in coronagraph images (Moore et al. 2015). This is an Alfvénic disturbance on the open field, and consequently it propagates outward at the Alfvén velocity. As pointed out in Sterling & Moore (2020), this velocity decreases between the corona, where the Alfvén velocity is  $\sim 1000 \text{ km s}^{-1}$ , and the location of PSP; Bale et al. (2019) report it to be  $\sim 100 \text{ km s}^{-1}$  at  $36.6 R_{\odot}$ . This leads to a contraction of the Alfvén pulse as it progresses outward, as indicated in panels (h)–(j) of Figure 3.

Via this process, the material ejected from the Sun in the jetting event, specifically along the spire, can become solar wind material if it gets out into the heliosphere (see Sterling & Moore 2020 for discussion of evidence that the jet material does indeed reach interplanetary space in some observed cases). At the very least, this can form some of the clumpy component (“flocculation”) of the solar wind (e.g., DeForest et al. 2016). Moreover, it can explain the presence of the “plasma jets” that are superimposed on the background Parker-like solar wind (Kasper et al. 2019; Raouafi et al. 2023), as well as the correlation between velocity microstreams and switchbacks (Neugebauer & Sterling 2021).

This also ties in the switchback structures with the solar wind in an intrinsic fashion: The jetting structures would produce the clumpy component of the solar wind. At the same time, the jetting structures would launch Alfvén wave pulses onto open field lines that stretch into the heliosphere, and along those field lines those pulses would evolve into kinks in the field lines that would appear as switchbacks.

Switchbacks in the solar wind seem to cluster on preferential size scales about the size of supergranules (Bale et al. 2021; Fargette et al. 2021), and there is also evidence of switchback widths corresponding to those of photospheric granules (Fargette et al. 2021). An average supergranule is about 30,000 km across, and this size is within about a factor of four of the size of the minifilaments that erupt to make jets, with substantial variation in both values. Similarly, microfilaments that might erupt to make some spicules are expected to be within about a factor of three or four of that of a typical granule (size  $\sim 1000 \text{ km}$ ). Therefore, jetting events preferentially of the sizes of coronal jets and of spicules could result in peaks in the observed widths of switchback clusters and individual switchbacks.

One possibility for these switchback-width and switchback-cluster-width size scales might follow from the distribution of size scales on which magnetic cancellation occurs in the photosphere. Convective motions in the photosphere occur over a range of size scales, but with peaks on the granule and supergranule scales (Hathaway et al. 2015). Magnetic fields

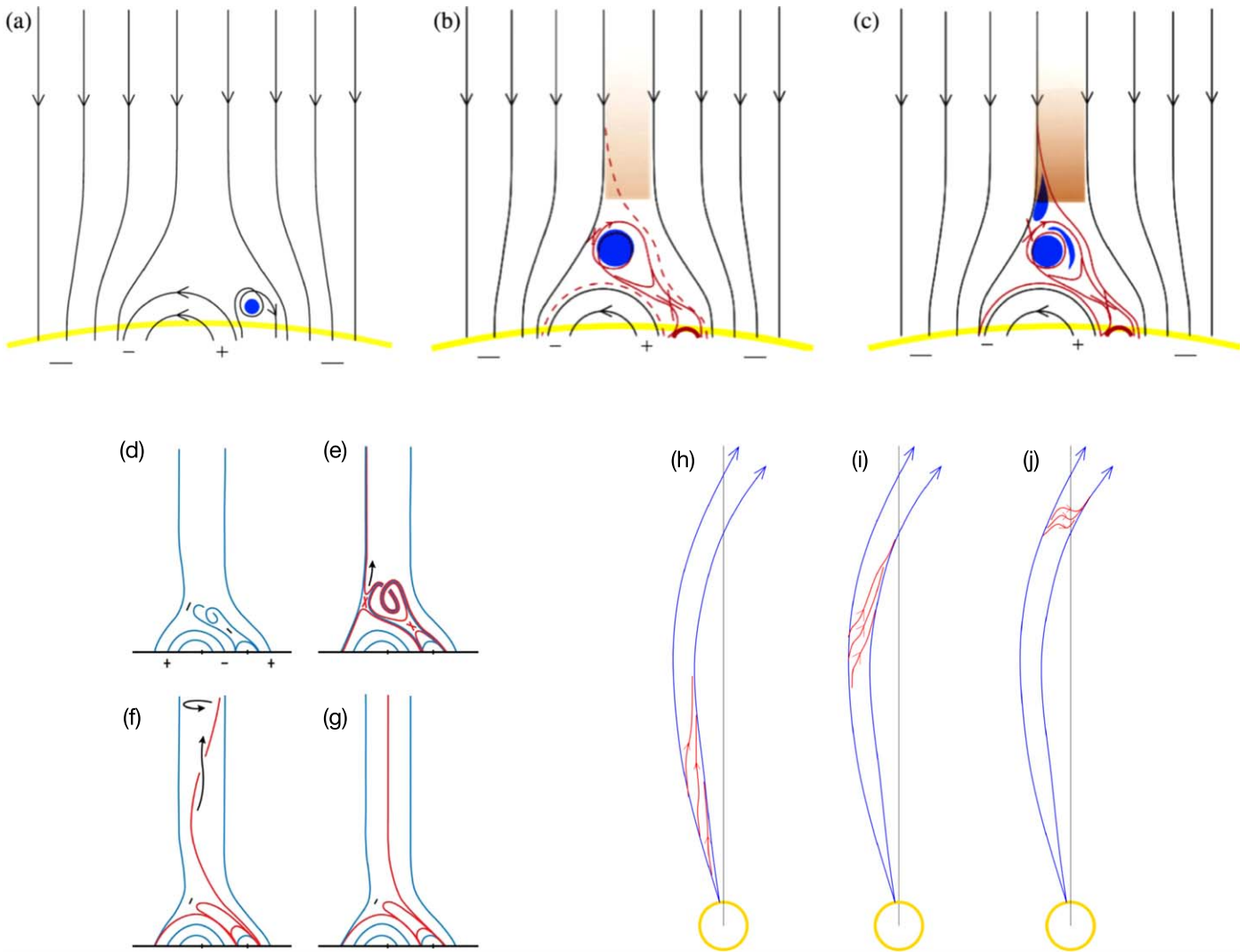


**Figure 3.** Summary of evolution of jetting events into switchbacks and solar wind. Panels (a)–(c) show the onset of jets in the minifilament eruption model. Black lines represent magnetic fields, with the background field a single polarity (negative) and open into the heliosphere. The blue circle represents a minifilament, and the looped black line around it indicates that it resides inside of a strongly sheared field or twisted magnetic flux rope. In panel (b) the minifilament is erupting, and its magnetic field is undergoing external reconnection (upper red cross) and internal reconnection (lower red cross). Red solid lines are heated reconnected field lines from the internal reconnection, dashed red lines are reconnected field lines from the external reconnection, the bright red arc represents the JBP, and the shaded region represents reconnection-heated material flowing outward and forming the jet spire. In panel (c), the external reconnection has progressed enough for the minifilament material to be also flowing out along the spire. This is a version of figures in Sterling et al. (2015) and Sterling et al. (2018), and further details appear in the text and captions of those papers. Panels (d)–(g) are versions of a figure in Moore et al. (2015) and show a continuation of the first three panels whereby the external reconnection of the erupting minifilament’s flux rope proceeds until the entire flux rope has opened up onto the open field. The twist of the flux rope escapes out into the corona, moving out as an Alfvénic twist pulse. Panels (h)–(j) show a modification of a figure in Sterling & Moore (2020). These show a continuation of the previous panels, with the magnetic twist wave forming a packet that propagates out into the heliosphere, steepening to become a switchback.

cluster around the edges of granules and of supergranules, pushed there by the horizontal flows of those convective structures. That could result in a preference for fields to shuffle around on those size scales, resulting in a preference for cancelations among opposite-polarity fields on those size scales. This could result in a preference for jetting events on these two size scales, meaning that coronal jets and spicule-sized jetting events are most common, resulting in the observed predominant width scales for switchbacks and switchback clusters (“patches”). It is unclear, however, whether coronal jets are frequent enough for eruptions of near-supergranule-sized minifilaments to explain the observed frequency of switchback patches. Therefore, perhaps a more likely explanation for these size scales is that most switchbacks result from small-scale eruptions that cause jetlet-sized and smaller jetlike features.

Because both jetlets (see Section 3) and spicules (e.g., Samanta et al. 2019) preferentially occur at network boundaries, switchbacks would also preferentially originate from those network boundaries; the network boundary is formed by supergranule motions, and so the network size reflects the supergranule size, and this could explain why switchbacks could be nearly continuously launched in bunches of the size scale of supergranules, resulting in the switchback patches on supergranule size scales.

## 7. Discussion

We have shown that CMEs, coronal jets, jetlets, and spicule-sized features are consistent with all forming as a consequence of the same basic mechanism on the Sun: eruption of magnetic flux ropes. The coronal jets and smaller features require the

anemone setup, while it is not clear that large flares require a magnetic null over the erupting location; Antiochos (1998) argues that it is required, but other works suggest that it is not essential (Joshi et al. 2017; Jiang et al. 2021).

In cases where an ejective eruption occurs inside of an anemone magnetic field configuration, one factor that determines whether a jetlike eruption occurs or a CME is ejected depends on how much of the erupting (mini)filament flux rope is eroded in the external reconnection with the surrounding open field. In the jet case, the field is (essentially) completely eroded away, so that no flux rope escapes: everything that is expelled, including the hot plasma and the cool minifilament material, escapes along the open coronal field. In the case of the CME, the erupting filament flux rope and its magnetic envelope contain enough flux that a remnant flux rope survives the external reconnection, and that remnant flux rope escapes into the heliosphere and forms the core of the CME. (There are also cases, however, where a jet forms where the erupting minifilament flux rope survives but is non-ejective, with the erupting flux rope remaining confined near the base of the jet. This is discussed in Sterling et al. 2022a.)

Thus, the features in Figure 2 that are small enough to survive as a jetting event rather than a CME are the ones that might contribute to the solar wind. Raouafi et al. (2023) suggest that jetlets are the main contributor to the solar wind, with the number of coronal jets being insufficient for the purpose. Our work here says that jetting events on a variety of size scales are available for contributing to the solar wind. This is consistent with the evidence put forward by Uritsky et al. (2023), who reached a similar conclusion through analysis of AIA images of outflows over 6 hr of continuous observations above a polar coronal hole. They found the mean size of the outflows, however, to be 3000–4000 km (and this is consistent with the findings of Kumar et al. 2023), which might be described as large jetlets or small coronal jets, according to Figure 2. Furthermore, the most commonly sized objects in their study (red open circle in Figure 2) are near the size of our plotted jetlet point (second-from-left black filled circle in Figure 2), and we deduce that the number of Uritsky et al. (2023) outflow events at any given time over the entire Sun is nearly identical to our estimate of the same quantity for jetlets in Figure 2. This supports that the events observed by Uritsky et al. (2023) largely originate from jetlet-sized coronal jetlike events.

Because the Alfvénic pulses imparted onto the open field would be longer close to the Sun and shorter farther away from the Sun (Figures 3(h)–(j)), on average the Alfvén packets would appear as less kinked magnetic features (or, smaller-rotation switchbacks) than after they travel farther from the Sun. As a result, they are less likely to be identified as switchbacks near the Sun than farther from the Sun. If features identified as switchbacks are not found (or, more exactly, if only very moderate magnetic field rotations are found) in the closest PSP perihelia, then this will not necessarily imply that switchbacks originate only in solar wind farther from the Sun; it could instead be that the seeds of those large-rotation switchbacks were launched by the Alfvénic pulses accompanying the jetting events, but those pulses have yet to evolve into larger-rotation switchbacks as described in Figures 3(h)–(j).

It is unclear to us how the plugs of plasma expelled in the jetting events could make it into the solar wind and maintain the hot temperature of solar wind material, as adiabatic cooling would be expected as the material disperses (Klimchuk 2012;

Sow Mondal et al. 2022). One concept deserving of consideration is the consequences of the twists put onto the open flux tubes by the erupting minifilaments.

We envision many of the erupting minifilaments leading to jetting to have twist on them at the time of the eruption. When this twist gets transferred to open field, the twist becomes an Alfvénic pulse, as discussed above and in Figure 3. These pulses will be of the form of a torsional Alfvénic twist, propagating outward along an open magnetic field. Hollweg et al. (1982) found that in some cases these propagating Alfvén waves can contribute to heating of the plasma through which they propagate. They found that as these Alfvén waves propagate up into the atmosphere, they can nonlinearly couple to fast- and slow-mode wave modes, which are compressive and can steepen into shocks and impart heating. They found much of this steepening to occur in the chromosphere, where the magnetic flux tube undergoes rapid expansion, leading to a density drop and increase in the Alfvén speed. This inspired much work trying to connect these waves with spicule production (Hollweg et al. 1982; Kudoh & Shibata 1999; Matsumoto & Shibata 2010).

For the minifilament eruption jetting mechanism, where (i.e., at what height in the atmosphere) twist will be imparted onto the open field depends on the size of the jetlike event. In Figure 2, only the smallest-size-scale events, representing the leftmost point (smallest-sized erupting filament-like features, leading to spicule-sized events) and not to the second point (representing the jetlets), would have external reconstructions in the chromosphere and thus be subject to the severe nonlinear effects discussed in Hollweg et al. (1982). These cases, however, are the most numerous, and therefore for them there is a valid question of whether this wave-mode coupling can result in plasma heating. A recent numerical simulation (Soler et al. 2019) using a train of such Alfvén waves and diffusive processes in the chromosphere (ohmic magnetic diffusion, or ambipolar diffusion, Khomenko & Collados 2012; and ion-neutral collisions) found only a small fraction of the energy to reach the corona;  $\sim 10^5$  erg cm<sup>-2</sup> s<sup>-1</sup>, but this might contribute to such heating. Other work, however, shows that the specific contribution of the Alfvén waves to heating of the solar atmosphere is dependent on the specific parameters of the flux tube and wave-launch conditions (Antolin & Shibata 2010). It would be of interest to see simulations representing the consequences of twists imparted in a manner representing the processes in Figure 3 and extending out to the location of PSP observations, to see whether heating via Alfvén wave-mode coupling to slow and fast modes leads to shocks that can heat the local solar wind plasma.

Karpen et al. (2017) undertook a 3D MHD simulation of a jet in a coronal hole field with an embedded bipole at the base of their calculation region. Their setup is similar to the coronal jet scenario presented in Sterling et al. (2015) and discussed in Section 2, with a minority magnetic polarity flux concentration surrounded by a broad region of majority flux and a null point in the corona above the minority-polarity flux. An important difference, though, is that they assumed symmetry to the system; in contrast, the Sterling et al. (2015) geometry is asymmetric, with one part of the anemone in a nonpotential state and holding a minifilament, while the rest of the anemone is roughly potential (see Figure 3(a)). In the Karpen et al. (2017) case, a jet results when a symmetric subsonic twist is imparted to the base of the setup, resulting in a puffing out of



the anemone base field, until a kink instability sets in, resulting in a jet traveling outward as a twist wave along the coronal field extending radially outward above the anemone’s null; this is different from the asymmetric minifilament/flux rope eruption deduced from our observations (Figures 3(b) and (c)).

In follow-up studies to Karpen et al. (2017), Uritsky et al. (2017) examined the structure and turbulent dynamics of the Karpen et al. (2017) simulated jet as it propagates out into the heliosphere, and Roberts et al. (2018) calculated predictions for what PSP will see from the resulting outward-propagating simulated jet. Uritsky et al. (2017) calculated that there would be a set of dynamic regions behind the outward-propagating leading edge of the jet, involving turbulent structures on various size scales (see Figure 14 of Uritsky et al. 2017). While these are interesting predictions, the manner in which the simulated jet is initiated differs from what we infer for jet onset based on our observations; our observations imply that the jet starts with the eruption of a minifilament/flux rope from an asymmetric magnetic anemone at the base of the jet spire field. It would be of interest if the analysis of Uritsky et al. (2017) and Roberts et al. (2018) could be carried out in a geometry that mimics more closely these observations, such as the simulation geometry of Wyper et al. (2017), to confirm whether the same far-from-Sun features develop. A further refinement would be to incorporate magnetic flux cancellation as the process for initiating the flux rope eruption in a simulation with a coronal topology such as that of Wyper et al. (2017).

Returning to the issue of observations of jets on various size scales, there is the possibility that it may be difficult to count smaller jets using imaging data alone. This is exemplified by two features, called “dark jets” and “inconspicuous jets.”

Young (2015) observed an on-disk coronal hole using spectral scans with the EUV Imaging Spectrometer (EIS) on Hinode. Doppler velocity maps of the region in the 195.12 Å Fe XII line revealed numerous transient localized regions of blueshifted upflows. Corresponding observations in AIA 193 Å images showed only either a weak counterpart or no signature at all at the upflow locations. He called these EIS features *dark jets* and found them to be as common as regular coronal hole jets, but with an intensity in AIA so low that the dark jets must have a mass flux 1 or 2 orders of magnitude lower.

In a similar fashion, Schwanitz et al. (2021) also looked at EIS spectral scans. They focused on 14 Doppler localized, transient EIS upflow regions and looked for counterparts in AIA EUV images and SXR images for the 5 of the 14 events observed with Hinode/XRT. They classified only one of the events as “obvious jets” and one as a “bright point with jet.” They classified seven as “small-scale brightenings/eruptions,” three as “bright points,” and two as “unclear.” Four of the 14 were at low latitude, allowing for comparison with HMI magnetograms. They report that three of these were “bright point” events and all three of these showed evidence for flux cancellation, and they say that the fourth event was unclear and showed no HMI feature.

Sterling et al. (2022b) looked more closely at the five Schwanitz et al. (2021) events having XRT data. One of those five was the one categorized as “obvious jets” in Schwanitz et al. (2021), but the other four were not classified as jets. But upon closely comparing dynamic motions in AIA and XRT images, Sterling et al. (2022b) concluded that all five were consistent with being coronal jets that were very inconspicuous in the images. The evidence for this includes that in all five

events they found evidence for eruption of a cool minifilament coinciding with the EIS upflow locations, and the sizes and near-eruption-onset-time speeds of those erupting minifilaments fall into the ranges of values for the same parameters found from confirmed coronal jets in previous studies (Sterling et al. 2015, 2022a). These erupting minifilaments were either confined to the jet-base location or perhaps ejective, but where the cool material becomes extremely tenuous low down so that it is not obvious beyond a smallish height; this perhaps explains why that material was not detected as a jet in most of the Schwanitz et al. (2021) cases. In addition, upon close inspection (including using difference images in one case), all five events showed a jet spire, and in four of the five cases where spire motion could be detected, that spire moved away from the JBP with time, which is also consistent with confirmed coronal jets (Baikie et al. 2022). All five of the Sterling et al. (2022b) events were near the north polar region. One of the five events, however, occurred at low enough latitude to allow comparisons with HMI, and those magnetograms were consistent with flux cancellation triggering that event.

The Young (2015) “dark jets” name applies to whatever it is that makes the EIS upflows, independent of whether they are true coronal jets. The “inconspicuous jets” described by Sterling et al. (2022b), on the other hand, are observed features that are strongly consistent with being true coronal jets but are hard to detect owing to their weak intensity in EUV and SXRs. Whether the Young (2015) dark jets are inconspicuous jets is not known at this time. One difference is the wavelength coverage inspected: Young (2015) investigated only one AIA channel (193 Å), while Sterling et al. (2022b) used four AIA channels (171, 193, 211, and 304 Å) and SXRs for their investigations. Therefore, it is unknown whether the dark jets are truly coronal jets. Similarly, it is unknown whether the remaining eight events not identified as jets in Schwanitz et al. (2021) (the nine other than the five studied by Sterling et al. 2022b, minus the one of those nine upflow location characterized as a “bright point with jet” in Schwanitz et al. 2021) are inconspicuous jets. But the Sterling et al. (2022b) study implies that the coronal jet mechanism is the cause of some upflows that are readily seen in EIS Doppler spectral scans but that are difficult to detect in EUV and SXR images. A key point is that this mechanism is responsible for more than just the jets that are obviously and easily detectable in AIA and EUV images. All five of the events studied in Sterling et al. (2022b) (which were selected from EIS Doppler data in Schwanitz et al. 2021) would have been too weak and feeble in XRT and/or EUV images to be selected as examples of jets in our previous jet studies (e.g., Moore et al. 2010, 2013; Sterling et al. 2015; Panesar et al. 2016b, 2018a; McGlasson et al. 2019; Sterling et al. 2022a).

### Acknowledgments

A.C.S. thanks N. Raouafi for stimulating discussions. We thank an anonymous referee for asking for more discussion of the observations of Uritsky et al. (2023) and for providing other helpful comments. A.C.S., R.L.M., and N.K.P. received funding from the Heliophysics Division of NASA’s Science Mission Directorate through the Heliophysics Supporting Research (HSR, grant No. 20-HSR20\_2-0124) Program and the Heliophysics Guest Investigators program. A.C.S. and R.L.M. were also supported through the Heliophysics System

Observatory Connect (HSOC, grant No. 80NSSC20K1285) Program. A.C.S. received additional support from the NASA/MSFC Hinode Project, and N.K.P. received additional support through a NASA SDO/AIA grant. We acknowledge the use of AIA data. AIA is an instrument on board SDO, a mission of NASA's Living With a Star program.

### ORCID iDs

Alphonse C. Sterling  <https://orcid.org/0000-0003-1281-897X>

Navdeep K. Panesar  <https://orcid.org/0000-0001-7620-362X>

Ronald L. Moore  <https://orcid.org/0000-0002-5691-6152>

### References

- Adams, M., Sterling, A. C., Moore, R. L., & Gary, G. A. 2014, *ApJ*, **783**, 11
- Antiochos, S. K. 1998, *ApJL*, **502**, L181
- Antolin, P., & Shibata, K. 2010, *ApJ*, **712**, 494
- Baikie, T. K., Sterling, A. C., Moore, R. L., et al. 2022, *ApJ*, **927**, 79
- Bale, S. D., Badman, S. T., Bonnell, J. W., et al. 2019, *Natur*, **576**, 237
- Bale, S. D., Horbury, T. S., Velli, M., et al. 2021, *ApJ*, **923**, 174
- Berghmans, D., Auchère, F., Long, D. M., et al. 2021, *A&A*, **656**, L4
- Chen, H., Hong, J., Yang, B., Xu, Z., & Yang, J. 2020, *ApJ*, **902**, 8
- Chen, H., Zhang, J., & Ma, S. 2012, *RAA*, **12**, 573
- Chen, P. F. 2011, *LRSP*, **8**, 1
- Chitta, L. P., Zhukov, A. N., Berghmans, D., et al. 2023, *Sci*, **381**, 867
- Curdtt, W., Tian, H., & Kamio, S. 2012, *SoPh*, **280**, 417
- DeForest, C. E., Matthaeus, W. H., Viall, N. M., & Cranmer, S. R. 2016, *ApJ*, **828**, 66
- Fargette, N., Lavraud, B., Rouillard, A. P., et al. 2021, *ApJ*, **919**, 96
- Hathaway, D. H., Teil, T., Norton, A. A., & Kitiashvili, I. 2015, *ApJ*, **811**, 105
- Hinode Review Team, Khalid, A. J., Patrick, A., et al. 2019, *PASJ*, **71**, R1
- Hollweg, J. V., Jackson, S., & Galloway, D. 1982, *SoPh*, **75**, 35
- Hong, J., Jiang, Y., Yang, J., et al. 2013, *RAA*, **13**, 253
- Iijima, H., & Yokoyama, T. 2017, *ApJ*, **848**, 38
- Jiang, C., Feng, X., Liu, R., et al. 2021, *NatAs*, **5**, 1126
- Joshi, B., Thalmann, J. K., Mitra, P. K., Chandra, R., & Veronig, A. M. 2017, *ApJ*, **851**, 29
- Joshi, N. C., Nishizuka, N., Filippov, B., Magara, T., & Tlatov, A. G. 2018, *MNRAS*, **476**, 1286
- Kamio, S., Curdt, W., Teriaca, L., Inhester, B., & Solanki, S. K. 2010, *A&A*, **510**, 1
- Karpen, J. T., DeVore, C. R., Antiochos, S. K., & Pariat, E. 2017, *ApJ*, **834**, 62
- Kasper, J. C., Bale, S. D., Belcher, J. W., et al. 2019, *Natur*, **576**, 228
- Khomenko, E., & Collados, M. 2012, *ApJ*, **747**, 87
- Klimchuk, J. A. 2012, *JGR*, **117**, A12102
- Kotani, Y., & Shibata, K. 2020, *PASJ*, **72**, 75
- Kudoh, T., & Shibata, K. 1999, *ApJ*, **514**, 493
- Kumar, P., Karpen, J. T., Uritsky, V. M., et al. 2022, *ApJ*, **933**, 21
- Kumar, P., Karpen, J. T., Uritsky, V. M., et al. 2023, *ApJL*, **951**, L15
- Liu, J., Wang, Y., & Erdélyi, R. 2019, *FrASS*, **6**, 44
- Martínez-Sykora, J., De Pontieu, B., Hansteen, V. H., et al. 2017, *Sci*, **356**, 1269
- Matsumoto, T., & Shibata, K. 2010, *ApJ*, **710**, 1857
- McGlasson, R. A., Panesar, N. K., Sterling, A. C., & Moore, R. L. 2019, *ApJ*, **882**, 16
- Moore, R. L., Cirtain, J. W., Sterling, A. C., & Falconer, D. A. 2010, *ApJ*, **720**, 757
- Moore, R. L., Sterling, A. C., Cirtain, J. W., & Falconer, D. A. 2011, *ApJL*, **731**, L18
- Moore, R. L., Sterling, A. C., Falconer, D. A., & Robe, D. 2013, *ApJ*, **769**, 134
- Moore, R. L., Sterling, R. L., & Falconer, D. A. 2015, *ApJ*, **806**, 11
- Moore, R. L., Sterling, R. L., & Panesar, N. K. 2018, *ApJ*, **859**, 3
- Morton, R. J., Srivastava, A. K., & Erdélyi, R. 2012, *A&A*, **542**, A70
- Muglach, K. 2021, *ApJ*, **909**, 133
- Neugebauer, M., & Sterling, A. C. 2021, *ApJL*, **920**, L31
- Nisticò, G., Bothmer, V., Patsourakos, S., & Zimbardo, G. 2009, *SoPh*, **259**, 87
- Panesar, N. K., Sterling, A. C., & Moore, R. L. 2016a, *ApJL*, **822**, L7
- Panesar, N. K., Sterling, A. C., & Moore, R. L. 2017, *ApJ*, **844**, 131
- Panesar, N. K., Sterling, A. C., & Moore, R. L. 2018a, *ApJ*, **853**, 189
- Panesar, N. K., Sterling, A. C., Moore, R. L., et al. 2018b, *ApJ*, **868**, L27
- Panesar, N. K., Sterling, A. C., Moore, R. L., et al. 2019, *ApJL*, **887**, L8
- Panesar, N. K., Sterling, A. C., Moore, R. L., & Chakrapani, P. 2016b, *ApJL*, **832**, L7
- Panesar, N. K., Tiwari, S. K., Berghmans, D., et al. 2021, *ApJL*, **921**, L20
- Panesar, N. K., Tiwari, S. K., Moore, R. L., Sterling, A. C., & De Pontieu, B. 2022, *ApJ*, **939**, 25
- Paraschiv, A. R., & Donea, A. 2019, *ApJ*, **873**, 110
- Paraschiv, A. R., Donea, A., & Leka, K. D. 2020, *ApJ*, **891**, 149
- Paraschiv, A. R., Donea, A. C., & Judge, P. G. 2022, *ApJ*, **935**, 172
- Patsourakos, S., Pariat, E., Vourlidas, A., Antiochos, S. K., & Wuelser, J. P. 2008, *ApJL*, **680**, L73
- Pike, C. D., & Mason, H. E. 1998, *SoPh*, **182**, 333
- Rachmeler, L. A., Winebarger, A. R., Savage, S. L., et al. 2019, *SoPh*, **294**, 174
- Raouafi, N. E., Georgoulis, M. K., Rust, D. M., & Bernasconi, P. N. 2010, *ApJ*, **718**, 981
- Raouafi, N. E., Patsourakos, S., Pariat, E., et al. 2016, *SSRv*, **201**, 1
- Raouafi, N. E., & Stenborg, G. 2014, *ApJ*, **787**, 118
- Raouafi, N. E., Stenborg, G., Seaton, D. B., et al. 2023, *ApJ*, **945**, 28
- Roberts, M. A., Uritsky, V. M., DeVore, C. R., & Karpen, J. T. 2018, *ApJ*, **866**, 14
- Samanta, T., Tian, H., Yurchyshyn, V., et al. 2019, *Sci*, **366**, 890
- Savcheva, A., Cirtain, J., Deluca, E. E., et al. 2007, *PASJ*, **59**, 771
- Schieder, B. 2022, *FrASS*, **9**, 820183
- Schwanitz, C., Harra, L., Raouafi, N. E., et al. 2021, *SoPh*, **296**, 175
- Shen, Y. 2021, *RSPSA*, **477**, 217
- Shen, Y., Liu, Y., Su, J., & Deng, Y. 2012, *ApJ*, **745**, 164
- Shibata, K., Ishido, Y., Acton, L. W., et al. 1992, *PASJ*, **44**, L173
- Shibata, K., & Magara, T. 2011, *LRSP*, **8**, 6
- Shibata, K., Nakamura, T., Matsumoto, T., et al. 2007, *Sci*, **318**, 1591
- Shibata, K., & Uchida, Y. 1986, *SoPh*, **178**, 379
- Shimojo, M., & Shibata, K. 2000, *ApJ*, **542**, 1100
- Soler, R., Terradas, J., Oliver, R., & Ballester, J. L. 2019, *ApJ*, **871**, 3
- Sow Mondal, S., Klimchuk, J. A., & Sarkar, A. 2022, *ApJ*, **937**, 71
- Sterling, A. C. 2000, *SoPh*, **196**, 79
- Sterling, A. C. 2018, *JPhCS*, **1100**, 012024
- Sterling, A. C. 2021, in *Solar Physics and Solar Wind*, ed. N. E. Raouafi & A. Vourlidas, Vol. 258 (New York: Wiley), 221
- Sterling, A. C., Harra, L. K., & Moore, R. L. 2010, *ApJ*, **722**, 1644
- Sterling, A. C., & Moore, R. L. 2016, *ApJL*, **828**, L9
- Sterling, A. C., & Moore, R. L. 2020, *ApJL*, **896**, L18
- Sterling, A. C., Moore, R. L., Falconer, D. A., & Adams, M. 2015, *Natur*, **523**, 437
- Sterling, A. C., Moore, R. L., & Panesar, N. K. 2018, *ApJ*, **864**, 68
- Sterling, A. C., Moore, R. L., & Panesar, N. K. 2022a, *ApJ*, **927**, 127
- Sterling, A. C., Moore, R. L., & Panesar, N. K. 2024, *ApJ*, **960**, 109
- Sterling, A. C., Moore, R. L., Panesar, N. K., et al. 2023, *FrASS*, **10**, 49
- Sterling, A. C., Moore, R. L., Samanta, T., & Yurchyshyn, V. 2020, *ApJL*, **893**, L45
- Sterling, A. C., Schwanitz, C., Harra, L. K., et al. 2022b, *ApJ*, **940**, 85
- Uritsky, V. M., Karpen, J. T., Raouafi, N. E., et al. 2023, *ApJL*, **955**, L38
- Uritsky, V. M., Roberts, M. A., DeVore, C. R., & Karpen, J. T. 2017, *ApJ*, **837**, 123
- van Ballegoijen, A. A., & Martens, P. C. H. 1989, *ApJ*, **343**, 971
- Veronig, A., Temmer, M., Hanslmeier, A., Otruba, W., & Messerotti, M. 2002, *A&A*, **382**, 1070
- Wang, Y. M., Sheeley, N. R., Jr., et al. 1998, *ApJ*, **508**, 899
- Wyper, P. F., Antiochos, S. K., & DeVore, C. R. 2017, *Natur*, **544**, 452
- Yashiro, S., Gopalswamy, N., Michalek, G., et al. 2004, *JGRA*, **109**, A07105
- Yokoyama, T., & Shibata, K. 1995, *Natur*, **375**, 42
- Young, P. R. 2015, *ApJ*, **801**, 124
- Young, P. R., & Muglach, K. 2014a, *PASJ*, **66**, 12
- Young, P. R., & Muglach, K. 2014b, *SoPh*, **289**, 3313
- Zhelyazkov, I., & Chandra, R. 2018, *MNRAS*, **478**, 5505
- Zhukov, A. N., Mierla, M., Auchère, F., et al. 2021, *A&A*, **656**, A35